Engineering Transactions, **70**(2): 183–199, 2022, doi: 10.24423/EngTrans.1311.20220602
Institute of Fundamental Technological Research Polish Academy of Sciences (IPPT PAN)
Université de Lorraine • Poznan University of Technology

Technical Note

A Proposal of a Novel Geometrical Measure of Material Effort

Krzysztof WACŁAWIAK

Silesian University of Technology
Department of Materials and Technologies
Katowice, Poland

e-mail: krzysztof.waclawiak@polsl.pl

A stress tensor may be presented as a surface delimited by a stress vector located at angles α_1, α_2, α_3 in relation to axes x, y, z. Geometrically, it outlines a domain and is linked to the loading. In this study, the area of such a surface and the volume of the domain were determined, along with their cross-sections with reference to areas and circumferences. Different stresses were also compared. This article presents cases of uniaxial, biaxial, triaxial tension and pure shear for an isotropic solid body. The analysis of a stress tensor in this conceptual work does not involve any material features, yet yields interesting results, particularly in the case of pure shear and uniaxial tension.

Key words: stress tensor; geometrical representation; material effort hypotheses.

1. Introduction

A stress tensor is an example of a second-order tensor. Referring to its graphical representation, a set of interdependencies is observed. Namely, if a scalar as a tensor of zero order is presented as a point in a coordinate system, and a vector as a first-order tensor is shown as a line segment with a definite direction, then a second-order tensor should have its graphical representation as a surface. A basic transformation Eq. (1.1) for principal stresses can be used for the calculations of the normal stress acting on a surface defined by direction cosines in relation to axes of principal stresses, including the angles between the surface normal and the coordinate axes α_1, α_2, α_3, Eq. (1.2) (Fig. 1):

$$\sigma_\mu = \sigma_1 \cos^2(\alpha_1) + \sigma_2 \cos^2(\alpha_2) + \sigma_3 \cos^2(\alpha_3), \tag{1.1}$$

where the direction cosines are calculated from a geometrical relationship:

$$\cos^2(\alpha_1) + \cos^2(\alpha_2) + \cos^2(\alpha_3) = 1. \tag{1.2}$$

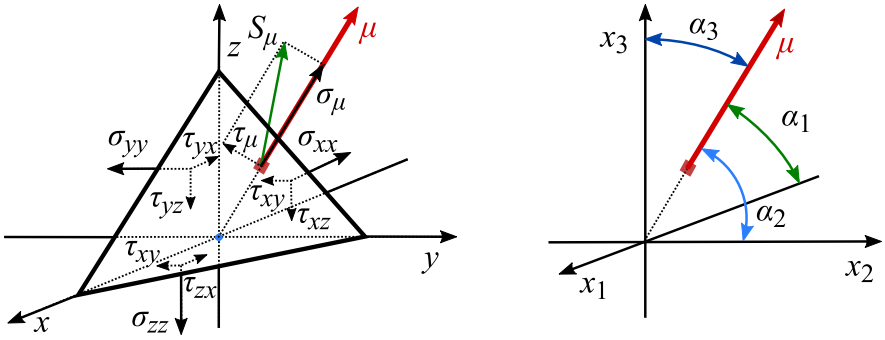

FIG. 1. A schematic presentation of analysed angles and their stress relation.

The concept of a graphical presentation of a stress tensor is not new, and was presented decades ago, for instance, in Polish literature [1]. Nowadays, handbooks on solid mechanics also include chapters where such an approach is shown [2]. These references define the surface in question as Cauchy's stress quadric, Eq. (1.3), [1] or Lame's stress ellipsoid, Eq. (1.4) [3]. In the case of principal stresses of the same signs, these equations produce simple shapes. For a triaxial uniform tensile strain-stress distribution, the latter is presented by a sphere, which with $\sigma_1 \neq \sigma_2 \neq \sigma_3$ changes into a triaxial ellipsoid with different diameters, and with $\sigma_1 \neq \sigma_2$ and $\sigma_2 = \sigma_3$ acquires the shape of a spheroid. When a plane stress state is present, the surface is reduced to a circle or ellipse, and eventually, it is shown as a line segment of uniaxial tension:

$$\sigma_1 x_1^2 + \sigma_2 x_2^2 + \sigma_3 x_3^2 = \pm \left(x_1^2 + x_2^2 + x_3^2\right)^{3/2}, \tag{1.3}$$

$$\left(\frac{\sigma_x}{\sigma_1}\right)^2 + \left(\frac{\sigma_y}{\sigma_2}\right)^2 + \left(\frac{\sigma_z}{\sigma_3}\right)^2 = 1. \tag{1.4}$$

2. THEORY SECTION

Since Galileo's pioneer work on the strength of materials, scholars have been trying to determine the strength of structural members under simple and complex loading conditions and afterwards compare the damaging forces or torques. Such a comparison was an attempt to define the first and subsequent theories of material effort. Basically, each theory has been verified against empirical data in tests for tension or compression under uniaxial, biaxial, and pure shear. Uniaxial testing is still the most universal. Therefore, its ultimate or yield strengths are the values to which the equivalent theoretical stress or strain are compared. Practically, out of convenience and experience, stress is preferred to strain.

Several theories have been proposed and applied, some of which are more appropriate for ductile materials, while others for brittle materials. Historically [4], theories were developed for isotropic materials and later for more demanding and difficult orthotropic or anisotropic ones. A group of classical theories includes the oldest ones like maximum normal stress, maximum shear strain, Coulomb and Huber-von Mises criteria.

The classic formulation of theories of material effort began a few centuries ago with the oldest material effort hypothesis considered to be Galileo's claim that material's performance was only limited by its tensile strength. Later, it was rejected and replaced by Lame's and Rankine's statement that both loadings, in tension and compression, defined material strength. While these scientists always thought of principal stresses, the hypotheses by Mariotte and then by Poncelet and Saint-Venant focused not on stress but strain. Those new approaches included more transformation and material properties, such as Poisson's ratio, and considered more brittle materials under compression. To some extent, they were later altered by Grashof in order to adapt them for ductile materials; unfortunately, they then lost their applicability for brittle materials. Another condition, still in use nowadays, was formulated by Coulomb in the 17th century and afterwards adapted by Guest and Tresca in the 19th century. Today it is classified as the Coulomb-Tresca hypothesis and is used for ductile materials. Both researchers focused on the shear stress component and its maximum value as the limiting value for material effort. This hypothesis assumes that the limit stress, either yield or ultimate, is the same for tension and compression. At the beginning of the 20th century, another theory was formulated by Huber [5] and von-Misses, which is today a widely accepted hypothesis, originally inspired by Huber, who suggested that material effort is measured by specific work of strain and eventually brought attention to distortion strain energy and its relation to the second invariant of deviatoric stress. As such, it is best fitted for ductile materials such as certain metals and their alloys. A few more researchers have contributed to the now used formula of this hypothesis, thus extending its name to the Maxwell-Huber-Hencky-von Mises theory.

The 20th century brought a series of advanced formulations of material effort hypotheses, extending the previous ones and adapting them to orthotropic and anisotropic materials and composites. It began with empirical corrections for isotropic materials that show diverse properties under compression and tension. They [6] were formulated by Burzynski and Nadai, Schleicher, and Burzynski [7] again, Yagn, Balandin, Drucker and Prager, Matsuura, Hu and Pae, Pervushi, Gol'denblat and Kopnov. Other researchers, e.g., Geniev and Kissyuk, Tarasenko, Yagn and Vinogradov, and Hill [8] introduced modifications or adopted new approaches. To sum up, a large number of researchers have con-

tributed to the development of modern understanding of material effort. While the rapid development of numerical technology has slowed down this research, new materials require novel methods for descriptions of their behaviour and modifications of the proposed models. An example of an analysis based on Burzynski's theory is presented in [9], and its modification in another paper [10]. A general implicit model for an orthotropic material is presented in a paper published in 2003 [11]. An attempt to bring forward a new criterion is presented in a recent paper [12], whose authors analyse an initially anisotropic material and compare its yield criteria with modified equations for isotropic materials.

2.1. Assumptions of analysis

It is convenient to analyse a stress tensor at a point of the body expressed by its principal stresses. Another option is to calculate a large number of related normal stress vectors (1.1) and present them as a cloud of points, with their coordinates as components of this normal stress vector in x, y, and z coordinates. Such an approach has a great advantage since, for each case of analysed stress tensor at the point of the body, the cloud of points enables representation of a surface that outlines a domain in space. Thus, the areas of the different surfaces referring to different stresses can be calculated, and different stress states may be compared.

This work presents the results of an analysis of four cases, namely: triaxial tension, biaxial tension, uniaxial tension and pure shear. In order to graphically represent these typical stress states, exemplary calculations were conducted. In all cases, the principal stresses were equal to ± 1 (without a unit). It has been assumed that $\sigma_1 = \sigma_x$, $\sigma_2 = \sigma_y$, and $\sigma_3 = \sigma_z$. These cases were described by the volume and surface of the domain enclosed by a closed surface. Additionally, its cross-section was described with regard to its surface area and circumference. There are three ways of representing such domains and analysing individual cases either by:

(i) generation of a cloud of points,
(ii) the revolution of a line segment around a selected axis or
(iii) by defining parametrical or implicit equations and implementing modern software to produce the surface that encloses the analysed figure.

Admittedly, the points obtained in method (i) do not form a surface but a database of coordinates. Therefore, calculations of the areas of tensor 'surfaces' presented in this paper are complex (Fig. 2). The second method offers an easier solution. Current software enables the delineation of a surface area and the calculation of its parameters. In this study, Ansys software was used with its DesignModeler geometry representations.

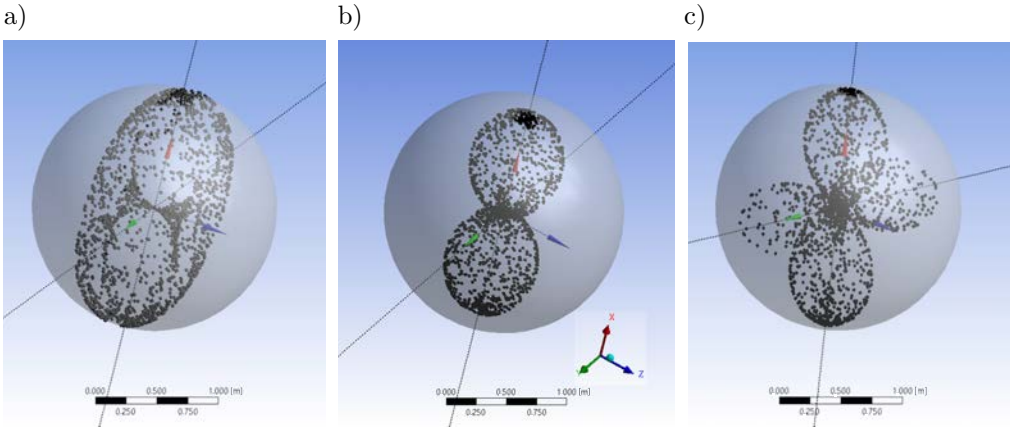

FIG. 2. Graphical representation of a cloud of points referring to normal stress tensor inside a sphere of triaxial tension: a) biaxial, b) uniaxial, c) pure shear.

3. Analysed cases of loading

The domains obtained in each analysed case of loading are presented below. The four pictures (Figs. 3–6) show the whole domain, one-half of the domain and its cross-section along the x-y-plane. Some figures are accompanied by tables generated by the software and present the calculated parameters of their volumes, areas, and/or lengths of the domain, its surface or circumference, respectively. In Fig. 6, a case of pure shear is presented, where $\sigma_1 = -\sigma_2$ and $\sigma_3 = 0$.

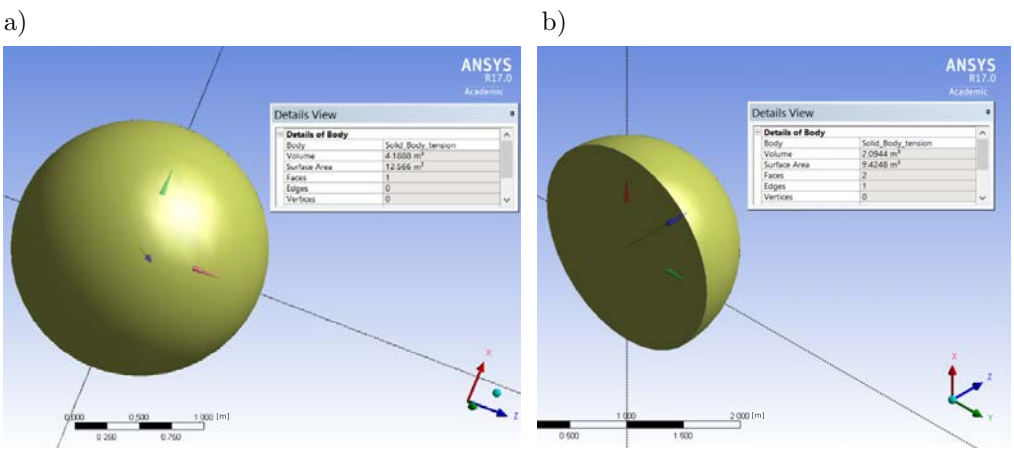

FIG. 3. The case of triaxial tension: a) isometric view of the whole domain, b) isometric view of one-half of the domain.

a) b)

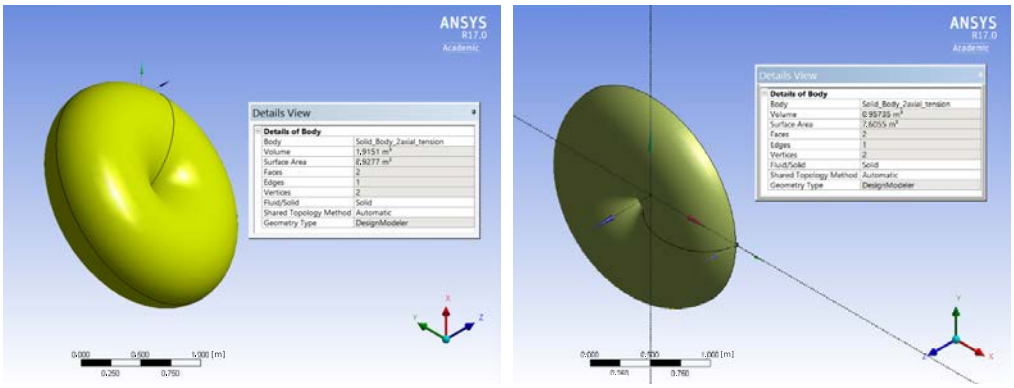

FIG. 4. The case of biaxial tension: a) isometric view of the whole domain, b) isometric view of one-half of the domain (cut along the x-y-plane).

a) b)

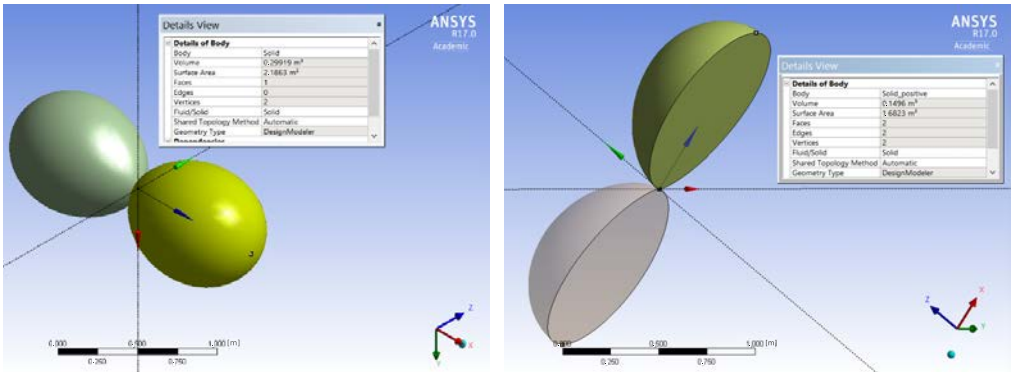

c)

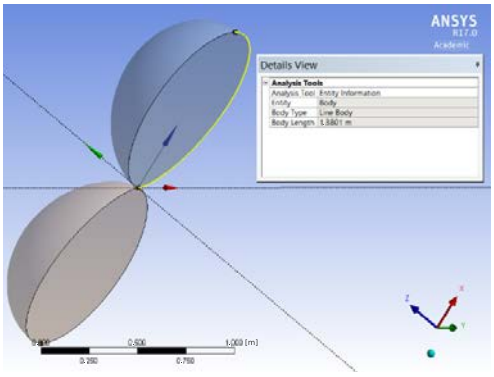

FIG. 5. The case of uniaxial tension: a) isometric view of the whole domain, b) isometric view of one-half of the domain, c) 1/4 of the circumference.

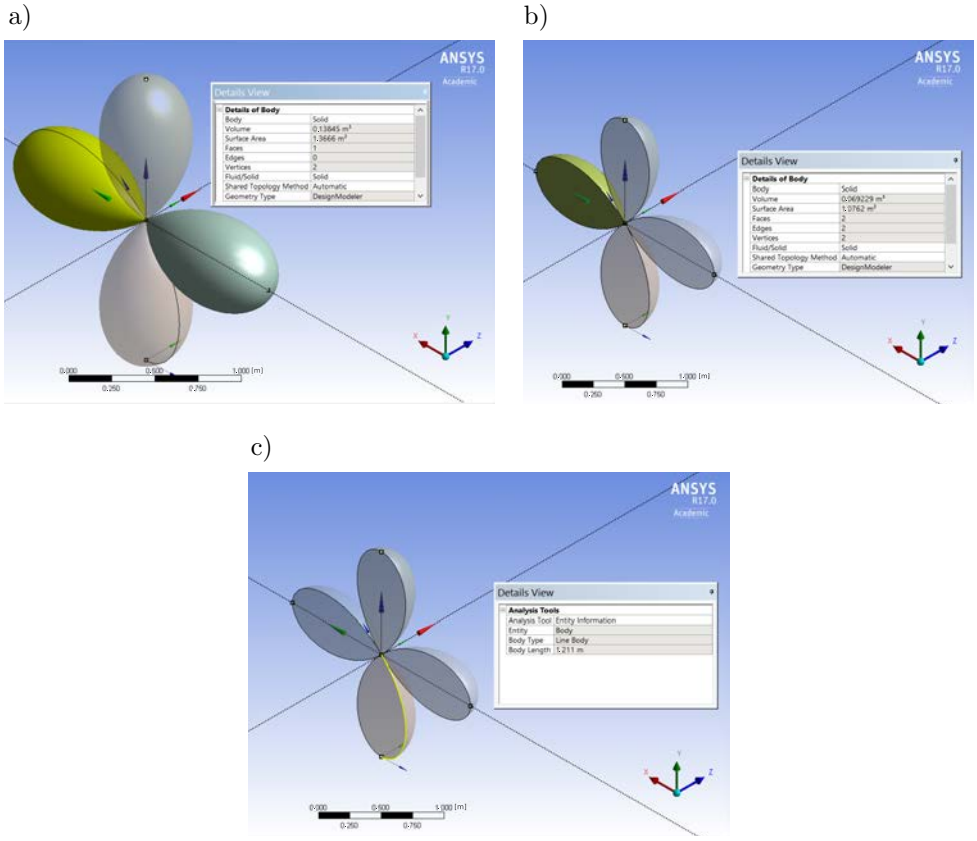

FIG. 6. The case of pure shear: a) isometric view of the whole domain, b) isometric view of one-half of the domain, c) 1/8 of the circumference.

The summary of the numerical results is shown in Tables 1 and 2.

Table 1. Basic geometrical features of the domains (V – volume, S – surface area).

Loading	Principal stress σ_i ($i = 1, 2, 3$)	Whole domain		One-half of the domain cut along the x-y-plane (surface includes the cross-section)	
		V	S	V	S
Triaxial tension (Fig. 3)	1; 1; 1	4.189	12.567	2.095	9.424
Biaxial tension (Fig. 4)	1; 1; 0	1.915	8.928	0.957	7.605
Uniaxial tension (Fig. 5)	1; 0; 0	$0.598 = 2 \times 0.2992$	$4.373 = 2 \times 2.1863$	$0.299 = 2 \times 0.150$	$3.365 = 2 \times 1.682$
Pure shear (Fig. 6)	1; −1;0	$0.554 = 4 \times 0.1384$	$5.465 = 4 \times 1.3666$	$0.277 = 4 \times 0.0699$	$4.305 = 4 \times 1.076$

Table 2. Geometrical features of the cross-sections (S – surface area, L – circumference of the figure).

Loading	Principal stress σ_i ($i = 1, 2, 3$)	x-y-plane cross section of the domain	
		S	L
Triaxial tension (Fig. 3)	1; 1; 1	3.142	$6.283 = 2\pi R$ ($R = 1$)
Biaxial tension (Fig. 4)	1; 1; 0	3.142	$6.283 = 2\pi R$ ($R = 1$)
Uniaxial tension (Fig. 5)	1; 0; 0	1.178	$5.520 = 4 \times 1.3801$
Pure shear (Fig. 6)	1; −1; 0	1.572	$9.688 = 8 \times 1.211$

The coordinates of points were calculated by Eq. (3.1), with the use of Eq. (1.1), where α_1, α_2 ranged from 0 to 90°:

$$\sigma_{\mu,i} = \sigma_\mu \cos(\alpha_i), \qquad i = x, y. \tag{3.1}$$

In the next step, a file containing these coordinates was imported into the software in order to produce a line. Afterwards, the line was revolved along axis x or y, depending on the analysed case. Occasionally, the bodies were mirrored to appear on the negative side of the axes.

Under triaxial tension, the cross-section is identical to that obtained for biaxial tension when cut along the x-y-plane and has the shape of a circle.

As Figs. 3–6 show, all the analysed cases lead to different shapes of the delimiting surface. It seems interesting to investigate cases with identical geometrical parameters. Such a comparison may suggest an alternative method for material effort determination. In this method, the combined stress state is transformed into the equivalent stress state. Due to the simplicity and long experience in measurements, this is usually a uniaxial tension. For example, as literature on the mechanical behaviour of materials indicates [4], for isotropic materials and especially ductile metals and their alloys, that failure of tested specimens during pure shear happens at the normal stress $\tau \sim 0.6\sigma_r$ of the normal stress for a uniaxial tension test.

3.1. Comparisons of stress tensors of different stress states

As mentioned in the previous section, a set of geometrical parameters, including the volume, area and circumference, was gathered for each loading. An attempt has been made to calculate a few relative quantities, with pure shear and uniaxial tension being the most interesting cases.

Comparisons of different surfaces and their equivalent quantities are also used in other fields of science. In fluid mechanics, the non-dimensional Reynolds number is calculated based on the equivalent diameter, Eq. (3.2) [13]. For inter-

nal flow through pipes, it is the inner diameter. However, for tubes other than circular ones or with a flow along surfaces such as river beds, this diameter is determined using the following formula (A – area, U – the circumference of the fluid cross-sectional area):

$$d_e = \frac{4A}{U}. \tag{3.2}$$

A similar approach can be applied for gas radiation heat transfer, with a volume of gas enclosed within solid or imaginary borders or walls. For the gas with its determined volume and surface defined by borders, Eq. (3.3) is used (V – volume, F – area of the space filled with the gas) [14]:

$$L_o = \frac{4V}{F}. \tag{3.3}$$

Both equations enable transformations of any plane figures or three-dimensional domains to a circle diameter (d_e) or sphere diameter (L_o), respectively.

Firstly, for cases analysed and presented in Tables 1 and 2, and Figs. 3–6, both d_e and L_o are calculated and presented in Table 3.

Table 3. Parameters of equivalent geometrical quantities obtained in the analysis.

Loading	Principal stress σ_i ($i = 1, 2, 3$)	Equivalent quantity	
		d_e	L_o
Triaxial tension	1; 1; 1	2.00	1.33
Biaxial tension	1; 1; 0	2.00	0.86
Uniaxial tension	1; 0; 0	0.85	0.55
Pure shear	1; −1; 0	0.65	0.41

Equation (3.2) transforms a flat figure into a circle with a diameter equal to 2 ($2\sigma_{1,2} = 1$) for triaxial and biaxial tension, the analysed cross-section is along the x-y-plane and both figures are of the same shape. For uniaxial and pure shear, the diameters are different. Equation (3.3), by contrast, transforms a domain into a sphere for each case, yet results in a different numerical value. In view of the differences between the determined geometrical quantities, it was worth trying to find the principal stress for pure shear assuming equal geometrical parameters. Thus, the value of 0.57 was chosen, as reported in [4], to be normal stress leading to failure of isotropic materials, especially ductile metals and their alloys. A few trials were made, and their results are shown in Fig. 7 and summarised in Tables 4 and 5.

Neither the equivalent quantity nor the volume nor the surface alone showed to be the same as for uniaxial tension. Only the circumferences of the cross-sections of the domains equal to 5.52 are the same.

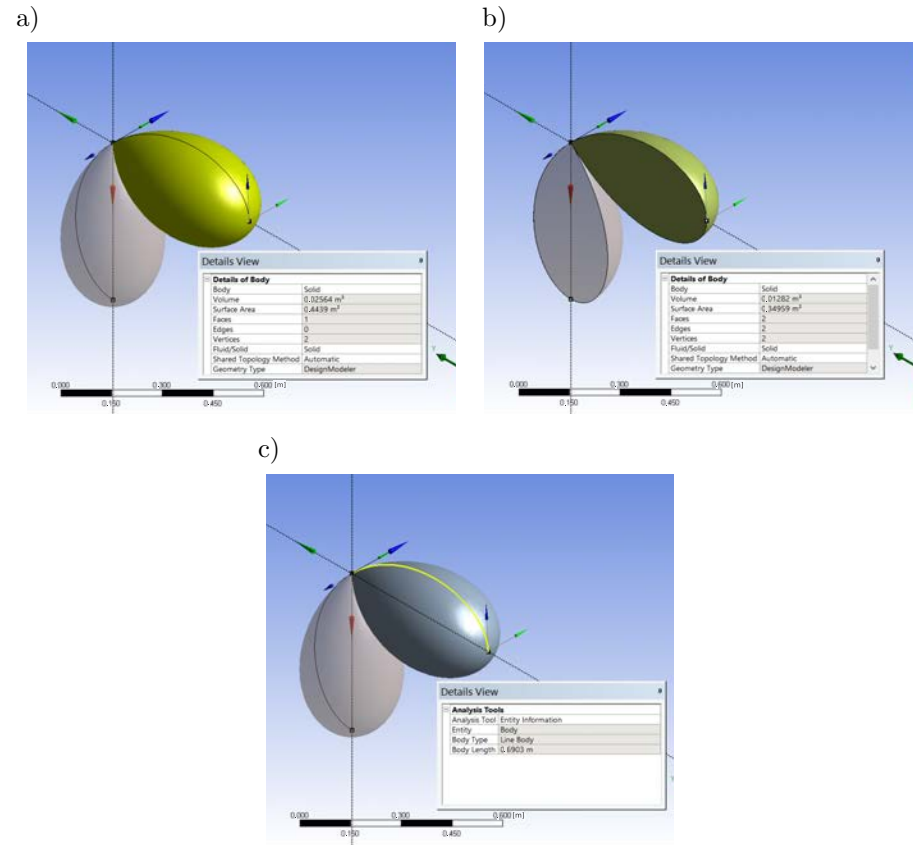

FIG. 7. "Equivalent" pure shear (only two parts of the entire domain are shown): a) isometric view of the whole domain, b) isometric view of a cross-section of the domain, c) 1/8 of the circumference.

Table 4. Basic geometrical features of the domains (V – volume, S – surface area).

Loading	Principal stress σ_i ($i = 1, 2, 3$)	Whole domain		One-half of the domain cut along the x-y-plane (surface includes the cross-section)	
		V	S	V	S
Uniaxial tension	1; 0; 0	$0.598 = 2 \times 0.2992$	$4.373 = 2 \times 2.1863$	$0.299 = 2 \times 0.150$	$3.365 = 2 \times 1.682$
Pure shear	0.57; −0.57; 0	$0.102 = 4 \times 0.0256$	$1.776 = 4 \times 0.4439$	$0.051 = 4 \times 0.0128$	$1.398 = 4 \times 0.346$

Three-dimensional analyses have been considered up to this point. As the results show, the circumference of the cross-section of the domains constitutes a comparative parameter. In the next section, a two-dimensional analysis is shown.

Table 5. Geometrical features of the domains' cross sections (S – surface area, L – circumference of the figure).

Loading	Principal stress σ_i ($i = 1, 2, 3$)	x-y-plane cross-section of the domain		Equivalent quantity	
		S	L	d_e	L_o
Uniaxial tension	1; 0; 0	1.178	**5.520** $= 4 \times 1.3801$	0.85	0.55
Pure shear	0.57; −0.57; 0	0.510	**5.522** $= 8 \times 0.6903$	0.37	0.23

It was assumed that $\sigma_1 = \sigma_y$, $\sigma_2 = \sigma_x$. In these planes, stress states components x and y of the normal stress Eq. (3.4) were calculated from Eqs. (3.5) and (3.6). The normal stresses were determined as follows:

$$\sigma_\mu = \sigma_1 \cos^2(\alpha_1) + \sigma_2 \sin^2(\alpha_1), \tag{3.4}$$

$$\sigma_{\mu,x} = \sigma_\mu \cos(\alpha_1), \tag{3.5}$$

$$\sigma_{\mu,y} = \sigma_\mu \sin(\alpha_1). \tag{3.6}$$

The lengths of different normal stress curves were calculated and next compared with the uniaxial tension by changing the input principal stresses. Figure 8 presents curves for the analysed cases along with the comparison of uniaxial tension of $\sigma_1(\sigma_x) = 1.0$ and equivalent, referring to its length, pure shear of $\sigma_1(\sigma_x) = |\sigma_2(\sigma_y)| = 0.58$. The direction angle α_1 ranged from 0 to 90°. The lengths of the curves defined by parametric Eqs. (3.4)–(3.6) are the same.

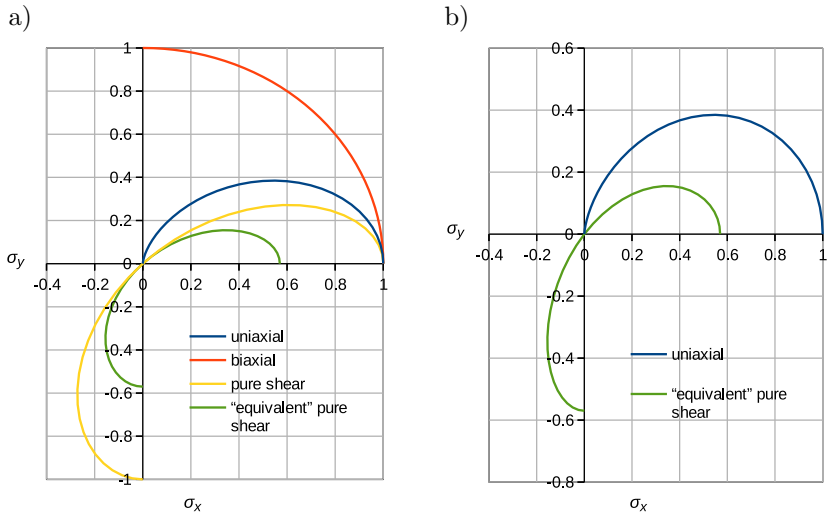

FIG. 8. Analysed cases of plane stress (a) and length identical to normal stress component (b) for uniaxial tension and pure shear.

A set of parametric equations for each case is shown in Table 6.

Table 6. Equations of the curves representing the analysed cases in parametric forms.

Loading	Principal stress σ_i $(i = 1, 2)$	Parametric equations of the curves for two-dimensional cases (plane stress) $\alpha_3 = \pi/2$ so geometrical relationship (1.2) reduces to the form: $1 = \cos^2(\alpha_1) + \cos^2(\alpha_2)$ and $\cos(\alpha_2) = \sin(\alpha_1)$	Range of α_1
Uniaxial tension	1; 0	$\sigma_\mu = \sigma_1 \cos^2(\alpha_1)$ $\sigma_{\mu,x} = [\sigma_1 \cos^2(\alpha_1)] \cos(\alpha_1)$ $\sigma_{\mu,y} = [\sigma_1 \cos^2(\alpha_1)] \sin(\alpha_1)$	$\langle 0;\ \pi/2 \rangle$
Biaxial tension	1; 1	$\sigma_\mu = \sigma_1 \cos^2(\alpha_1) + \sigma_2 \sin^2(\alpha_1)$ as $\sigma_1 = \sigma_2 = \sigma$ $\sigma_{\mu,x} = \sigma \cos(\alpha_1)$ $\sigma_{\mu,y} = \sigma \sin(\alpha_1)$	$\langle 0;\ \pi/2 \rangle$
Pure shear and "equivalent" pure shear	1; −1 and 0.57; −0.57	$\sigma_\mu = \sigma_1 \cos^2(\alpha_1) + \sigma_2 \sin^2(\alpha_1)$ as $\sigma_1 = -\sigma_2 = \sigma$ $\sigma_{\mu,x} = \sigma[\cos^2(\alpha_1) - \sin^2(\alpha_1)] \cos(\alpha_1)$ $\sigma_{\mu,y} = \sigma[\cos^2(\alpha_1) - \sin^2(\alpha_1)] \sin(\alpha_1)$	$\langle 0;\ \pi/2 \rangle$

Similarly, in Fig. 9, the cases of uniaxial tension and pure shear are presented, yet the direction angle α_1 varies within the range of 0 to 360°.

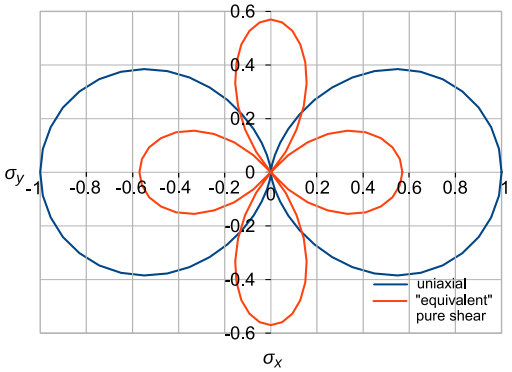

FIG. 9. Length-identical cases of normal stress for uniaxial tension and pure shear.

4. Discussion

As this proposal for a new diagnostic method demonstrates, a stress tensor at a selected point of the body can be graphically represented as a geometrical do-

main drawn on the basis of their principal stresses, followed by a cross-section of this domain. The sections along the principal stress planes were studied. The circumferences of the obtained cross-sectional figures were compared, and such comparisons introduced a feasible conversion from pure shear into uniaxial tension and vice versa.

Different hypotheses that address material effort describe material behaviour and final failure under combined stresses. Their goal is to transform complex stress conditions (referring to a system's response to loadings) into equivalent stress. Usually, this stress is defined as a simple uniaxial tension. In this way, combined stress is presented by one stress reduced value. The two basic criteria are determined by Coulomb-Tresca Eq. (4.1) and Huber-von Mises Eq. (4.2). The first one promotes maximum shear stress as the failure criterion, while the latter focuses on shear energy per unit of volume as a distortion energy criterion. In Table 7, the above-mentioned criteria are applied to the analysed cases and compared with those in the geometrical approach described in this article:

$$\sigma_{\text{equivalent}} = \sigma_{\max} - \sigma_{\min}, \tag{4.1}$$

$$\sigma_{\text{equivalent}} = \frac{\sqrt{(\sigma_1 - \sigma_2)^2 + (\sigma_2 - \sigma_3)^2 + (\sigma_3 - \sigma_1)^2}}{\sqrt{2}}. \tag{4.2}$$

Table 7. Set of Coulomb-Tresca and Huber-von Mises criteria along with geometrical approach for the analysed cases.

Loading	Principal stress σ_i ($i = 1, 2, 3$)	Coulomb-Tresca criterion	Huber-von Mises criterion	Geometrical comparison
Triaxial tension	1; 1; 1	0	0	1.14
Biaxial tension	1; 1; 0	1	1	1.14
Uniaxial tension	1; 0; 0	1	1	1
Pure shear	1; −1; 0	2	1.73	1.755

In order to perform such a comparison, the principal stress σ_1 was altered for uniaxial loading until the circumference of the cross-section presented in Fig. 4 or the length of the line in Fig. 7 reached the values shown in Table 2, column L, for the tri- and biaxial cases and the pure shear. Contrary to the two basic hypotheses, which show the equivalent stress equal to zero for triaxial tension, the geometrical approach leads to a non-zero value.

As yet, all these calculations have been carried out numerically, either by professional software or by using spreadsheets, applying differences Δx, Δy leading to $L = \Sigma\Delta L = \Sigma(\Delta x^2 + \Delta y^2)^{1/2}$. As the length of the curve can be calculated analytically by integrating, such an attempt was made as well. Equations (3.1)

and (3.4) present the normal stress using polar coordinates. For uniaxial tension, the length of the curve is determined by the following calculations:

$$L = \int_0^{\pi/2} \sqrt{\sigma_\mu^2 + (\sigma'_\mu)^2}\,\mathrm{d}\alpha = \sigma \int_0^{\pi/2} \sqrt{\cos^4(\alpha) + 4\sin^2(\alpha)\cos^2(\alpha)}\,\mathrm{d}\alpha \tag{4.3}$$

$$= \sigma \int_0^{\pi/2} \cos(\alpha)\sqrt{1 + 3\sin^2(\alpha)}\,\mathrm{d}\alpha = \sigma\sqrt{3}\int_0^1 \sqrt{\frac{1}{3} + t^2}\,\mathrm{d}t,$$

finally

$$L = \sqrt{3}\sigma \left\{ \frac{\sin(\alpha)}{2}\sqrt{\sin^2(\alpha) + \frac{1}{3}} + \frac{1}{6}\ln\left|\sin(\alpha) + \sqrt{\sin^2(\alpha) + \frac{1}{3}}\right| \right\}_0^{\pi/2}$$

or

$$L = \sqrt{3}\sigma \left\{ \frac{\sin(\alpha)}{2}\sqrt{\sin^2(\alpha) + \frac{1}{3}} + \frac{1}{6}\operatorname{arcsin\,h}(\sqrt{3}\sin(\alpha) \right\}_0^{\pi/2}.$$

If the limits of integration are 0 and 90° and $\sigma = 1$, the final length L of the curve equals 1.38. The same value, shown in Fig. 5, was integrated numerically by the graphical software. However, the case of pure shear cannot be easily integrated and expressed by means of elementary functions, as its similar conversion leads to an elliptic integral of the second type (Eq. (4.4)):

$$L = \int_0^{\pi/2} \sqrt{\sigma_\mu^2 + (\sigma'_\mu)^2}\,\mathrm{d}\alpha = \sigma \int_0^{\pi/2} \sqrt{\cos^2(2\alpha) + 4\sin^2(2\alpha)}\,\mathrm{d}\alpha \tag{4.4}$$

$$= \sigma \int_0^{\pi/2} \sqrt{1 + 3\sin^2(\alpha)}\,\mathrm{d}\alpha = \sigma\frac{1}{2}\int_0^1 \sqrt{1 + 3\sin^2(t)}\,\mathrm{d}t$$

$$= \sigma\frac{1}{2}\int_0^1 \sqrt{4 - 3\cos^2(t)}\,\mathrm{d}t = \sigma \int_0^{\pi/2} \sqrt{4 - 3\sin^2(\frac{\pi}{2} - \alpha)}\,\mathrm{d}\alpha$$

$$= -2\sigma\frac{1}{2}\int_0^{\pi/2} \sqrt{1 - \frac{3}{4}\sin^2(\beta)}\,\mathrm{d}\beta = -2\sigma\frac{1}{2}\int_0^{\pi/2} \sqrt{1 - k^2\sin^2(\beta)}\,\mathrm{d}\beta.$$

The negative value of "-2" in Eq. (4.4) originates from the substitution of variables, namely angle "t" with "α", and in the final form, is treated by

its modules (Eq. (4.6)). Presented in this equation, transformation (Eq. (4.4)) enables the calculation of this integral by a power series [15]:

$$\int_0^{\pi/2} \sqrt{1 - k^2 \sin^2(\theta)}\, \mathrm{d}\theta = E(k) = \frac{\pi}{2} \sum_{n=0}^{\infty} \left(\frac{(2n)!}{2^{2n}(n!)^2} \right)^2 \frac{k^{2n}}{1-2n}, \tag{4.5}$$

the sought-for curve length is determined by means of the following formula:

$$L \approx |-2|\, \sigma \left\{ \frac{\pi}{2} \sum_{n=0}^{N} \left(\frac{(2n)!}{2^{2n}(n!)^2} \right)^2 \frac{k^{2n}}{1-2n} \right\} = |-2|\, \sigma \frac{\pi}{2} \left\{ 1 - \left(\frac{1}{2}\right)^2 \frac{k^2}{1} - \left(\frac{3}{8}\right)^2 \frac{k^4}{3} - \ldots \right\}. \tag{4.6}$$

The obtained value is presented in a graph in Fig. 10 as a function of a number of terms taken in the sum. Assuming that the first six terms are sufficient for determination of the length, its numerical value equals 2.42 and is twice the length shown in Fig. 6. The reason for that is the difference in the integration limits. For the length calculated by integration, the limits are 0 and 90°, and the curve is presented in full in Fig. 8a, while the curve shown in Fig. 6 represents the limits of 0 and 45°.

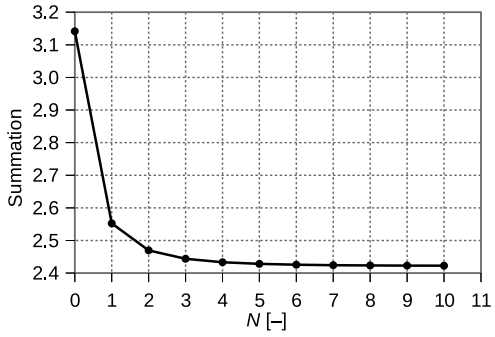

FIG. 10. Determined length of the analysed curve for pure shear by power series.

As the calculated length L has a dimension of stress, it is possible to determine a unit length "l" under uniaxial tension by Eq. (4.7):

$$L_{\text{uniaxial}} = \sigma_{\text{uniaxial}} l. \tag{4.7}$$

This quantity may be used to define equivalent stress under other loading patterns by means of the formula:

$$\sigma_{\text{equivalent}} = L_{\text{analysed}}/l. \tag{4.8}$$

Finally, it should be observed that the ratio of the determined length of the uniaxial tension and pure shear, namely 1.38 and 2.42, is 0.57. As this value is observed for isotropic materials and is confirmed by the determination based on the Huber-Misses criterion, it is important to highlight the results of the method outlined in this paper. These geometrical analyses have led to an observation that the Huber-Misses criterion for these cases may be derived on the basis of such an approach. A report on other cases of testing materials behaviour will be presented in a future publication.

5. Conclusions

The approach for a stress tensor analysis, as presented here, can be summarized by the following statement: each stress tensor is represented in a three-dimensional coordinate system as a domain, whose geometrical parameters such as volume, surface area, the cross-section and its surface area and the circumference can be compared. However, only the last one proved to be useful for finding equivalent stress states under pure shear, biaxial and uniaxial tension. The physical relation between the loading patterns and these analysed geometrical features, should one exist, is not conclusive and may be a subject of further study.

Such a method might be a new procedure for material effort comparisons and contribute to stress prediction methodology. It has proved to be feasible in typical comparisons between pure shear and uniaxial tension, as well as biaxial tension.

Such an approach can also be applied to domains formed by shear components of stress. Not only can a stress tensor be analysed this way but both normal and shear components of the strain tensor too. Extended analyses seem promising and will be presented in another publication. In the case in point, Poisson's ratio values as a property of material will influence the domains and their features.

References

1. Derski W., *Introduction to Continuum Mechanics* [in Polish: *Zarys mechaniki ośrodków ciągłych*], PWN, Warszawa, 1975.

2. Chaves E.W.V, *Notes on Continuum Mechanics*, Springer Science+Business Media, 2013.

3. Jakowluk A., Breczko T., *Continuum Mechanics* [in Polish: *Mechanika ośrodków ciągłych*], Wydawnictwo Politechniki Białostockiej, Białystok, 1985.

4. Jastrzębski P., Mutermilch J., Orłowski W., *Strength of Materials* [in Polish: *Wytrzymałość materiałów*], Arkady, Warszawa, 1986.

5. Huber T., Specific work of strain as a measure of material effort (translated from the original paper in Polish), *Archives of Mechanics*, **56**(3): 173–190, 2004.

6. Sendeckyj G.P., Empirical strength theories, [in:] *Testing for Prediction of Material Performance in Structures and Components*, R.S. Shane [Ed.], ASTM STP 515, American Society for Testing and Materials, pp. 171–179, 1972.

7. Burzyński W., Theoretical foundations of the hypotheses of material effort, *Engineering Transactions*, **56**(3): 269–305, 2008 [Translated from the original paper in Polish: Teoretyczne podstawy hipotez wytężenia, *Czasopismo Techniczne*, **47**: 1–41, 1929].

8. Hill R., A theory of the yielding and plastic flow of anisotropic metals, *Proceedings of the Royal Society of London. Series A. Mathematical and Physical Sciences*, **193**(1033): 281–297, 1948, doi: 10.1098/rspa.1948.0045.

9. Frąś T., Pęcherski R.B., Applications of Burzyński hypothesis of material effort for isotropic solids, *Mechanics and Control*, **29**(2): 45–50, 2010.

10. Pęcherski R.B., Szeptyński P., Nowak M., An extension of Burzyński hypothesis of material effort accounting for the third invariant of stress tensor, *Archives of Metallurgy and Materials*, **56**(2): 503–508, 2011, doi: 10.2478/v10172-011-0054-4.

11. Oller S., Car E., Lubliner J., Definition of a general implicit orthotropic yield criterion, *Computer Methods in Applied Mechanics and Engineering*, **192**(7–8): 895–912, 2003, doi: 10.1016/S0045-7825(02)00605-9.

12. Pęcherski R.B., Rusinek A., Fras T., Nowak M., Nowak Z., Energy-based yield condition for orthotropic materials exhibiting asymmetry of elastic range, *Archives of Metallurgy and Materials*, **65**(2): 771–778, 2020, doi: 10.24425/amm.2020.132819.

13. Kostowski E., *Heat Transfer* [in Polish: *Przepływ ciepła*], Wydawnictwo Politechniki Śląskiej, Gliwice, 1991.

14. Madejski J., *Theory of Heat Transfer* [in Polish: *Teoria wymiany ciepła*], Wydawnictwo Uczelniane Politechniki Szczecińskiej, Szczecin, 1998.

15. Oberhettinger F., Magnus W., *Implementation of Elliptic Functions in Physics and Technique* [in Polish: *Zastosowania funkcji eliptycznych w fizyce i technice*], PWN, Warszawa, 1963.

Received January 30, 2021; accepted version February 21, 2022.